CivilEng

MDPI

Article

Enhancing Deep Excavation Optimization: Selection of an Appropriate Constitutive Model

Bhim Kumar Dahal [1,†], Sandip Regmi [1,†], Kalyan Paudyal [1], Diwash Dahal [2] and Diwakar KC [3,4,*]

[1] Department of Civil Engineering, Pulchowk Campus, IOE, Tribhuvan University, Lalitpur 44600, Nepal; bhimd@pcampus.edu.np (B.K.D.); regmisndp95@gmail.com (S.R.); kalyanpaudyal@gmail.com (K.P.)
[2] Department of Civil Engineering, Southern Illinois University, Edwardsville, IL 62026, USA; geodahal@gmail.com
[3] Department of Civil and Environmental Engineering, University of Toledo, Toledo, OH 43606, USA
[4] Geotechnology LLC, 1780 Carillon Blvd, Cincinnati, OH 45240, USA
* Correspondence: dibakarkc@outlook.com
† These authors contributed equally to this work.

Abstract: To minimize the impact on nearby structures during deep excavations, choosing an appropriate soil constitutive model for analysis holds significant importance. This study aims to conduct a comparative analysis of various constitutive soil models—namely, the Mohr–Coulomb (MC) model, the hardening soil (HS) model, the hardening soil small strain (HSS) model, and the soft soil (SS) model—to identify the most suitable model for the lacustrine deposit. To implement these models, the soil's index properties and mechanical behavior were evaluated from undisturbed soil samples. The numerical simulation and verification of these properties were carried out by comparing the laboratory test results with the outcome of the finite element method; the most suitable constitutive soil model for the soil was identified as the HSS model. Upon analyzing the wall deflection and ground settlement profiles obtained from respective constitutive models, it was observed that the HS and HSS models exhibit similar characteristics and are well-suited for analyzing typical lacustrine soil. In contrast, the MC and SS models yield overly optimistic results with lower wall deflection and ground settlement and fail to predict realistic soil behavior. As a result, this research highlights the significance of selecting the appropriate constitutive soil model and refining the parameters. This optimization process contributes significantly to the design of support systems, enhancing construction efficiency and ensuring overall safety in deep excavation projects.

Keywords: deep excavation; finite element method; lacustrine soil; constitutive model

Citation: Dahal, B.K.; Regmi, S.; Paudyal, K.; Dahal, D.; KC, D. Enhancing Deep Excavation Optimization: Selection of an Appropriate Constitutive Model. *CivilEng* **2024**, *5*, 785–800. https://doi.org/10.3390/civileng5030041

Academic Editors: Angelo Luongo and Francesco D'Annibale

Received: 14 July 2024
Revised: 30 August 2024
Accepted: 7 September 2024
Published: 16 September 2024

1. Introduction

In cities with a high population density, such as Kathmandu, underground structures like basements, subways, metro stations, underground parking, etc., are necessary. Considering the rapid urbanization of such cities, underground structures have become more prominent due to a lack of space and the expensive land value. High-rise buildings for hotels, apartments, view towers, and commercial complexes with basements are increasing rapidly, and these require deep excavation for foundation. For traffic management in Kathmandu, the importance of underground parking, subways, railway tunnels, and metro stations is highlighted every day. Kathmandu Valley is composed of fluvial-lacustrine deposits [1–3]; therefore, deep excavation works should be conducted very carefully. During deep excavation in such soils, settlements of foundation, cracks in structures, and even the collapse of nearby structures might occur due to improper excavation and support systems. Settlements and a large sinkhole in a service lane and road collapse during excavation for the basement of a hotel in Naxal, Kathmandu; and settlements on nearby residential houses during the foundation excavation for an apartment in Sanepa, Kathmandu (see Figure 1), are some of the examples which directly affect daily life and the economy. These incidents

indicate that there is a lack of research, soil investigation, and analysis and poor practice during construction.

Figure 1. Failures in nearby structures: (**a**) Sanepa [4]; (**b**) Naxal, Kathmandu [5], during foundation excavation.

To lessen problems and make excavation more efficient, the identification of the mechanical behaviors of soil [6], the selection of appropriate constitutive soil models as per the performance evaluations of models, and the analysis and design of a support system as per a suitable constitutive soil model are crucial [7–11]. Moreover, it is difficult to identify the effect on the surroundings using conservative analytical methods [12,13].

Soil samples from Tukucha, Kathmandu Valley, are considered in this study. The study area is mainly composed of clayey, silty, sandy, and gravely sediments [1]. Earlier studies have reported the maximum thickness of sediments in the central part (550 m at Bhrikutimandap), which is close to the study area, and towards the southern part (>457 m at Harishidhi) of Kathmandu Valley [2].

1.1. Soil Constitutive Model

In geotechnical problems, the two concepts of effective and total stress analysis are widely used in numerical simulation. Generally, engineers prefer total stress analysis because the parameters used are more familiar and easier to determine with conventional soil tests, whereas effective stress analysis is preferred more by scientists due its solid theoretical formulations [14]. The effective stress-based constitutive soil models are the modified Cam Clay (MCC) model, the hardening soil (HS) model, and the hardening soil small strain (HSS) model which are widely used nowadays. Likewise, the Mohr–Coulomb (MC) model and the total undrained soft clay (USC) model are based on the total stress approach.

The MC model is highly recommended and mostly used for the initial analysis of geotechnical problems due to its simplicity as mentioned by Lim et al., 2010 [14]. This model is commonly used in deep excavation, the stability of dams, embankments, slopes, etc. Due to the consideration of the average stiffness, computation becomes comparatively fast, and a primary estimation of deformation can also be determined. The MC model is a linearly elastic and perfectly plastic model. The basic parameters required for the modeling

of the Mohr–Coulomb model are the Young's modulus (E), Poisson's ratio (ν), cohesion (c), friction angle (Φ), dilatancy angle (Ψ), and tension cut-off and tensile strength (σ_t).

The SS model, a Cam Clay type model, is most suitable to analyze the soft soils like normally consolidated clays, peats, etc. [15]. This model considers the associated flow on the cap surface so that the respective components can be easily identified (Figure 2a) [16]. This model gives the best result for primary compression. This model is not categorized under the Critical State Model (CSM) due to many upgradations in parameters. The input parameters required for this model are the modified compression index (λ^*), the modified swelling index (k^*), and the Mohr–Coulomb model failure parameters (c', Φ', Ψ). From an isotropic compression test along with isotropic unloading, the modified swelling index and modified compression index can be identified. The slope of the loading and unloading curve plotted between the logarithm of the mean stress and the volumetric strain give the value of λ^* and k^*, respectively, as shown in (Figure 2b). In the absence of an isotropic compression test, the parameters λ^* and k^* can be determined from a one-dimensional compression test. In this study, the relations given in Equations (1) and (2) below were used to determine the parameters λ^* and k^*.

$$\lambda^* = \frac{Cc}{2.3\ (1+e)}, k^* = \frac{Cs}{2.3\ (1+e)} \text{ or } \frac{2Cc}{2.3\ (1+e)} \quad (1)$$

$$\lambda^* = Cc/(2.3(1+e))$$

Alternately,

$$\lambda^* = \frac{\lambda}{(1+e)},\ k^* = \frac{k}{(1+e)} \quad (2)$$

where λ and k are the Cam Clay compression and swelling index, respectively, and 'e' is the void ratio.

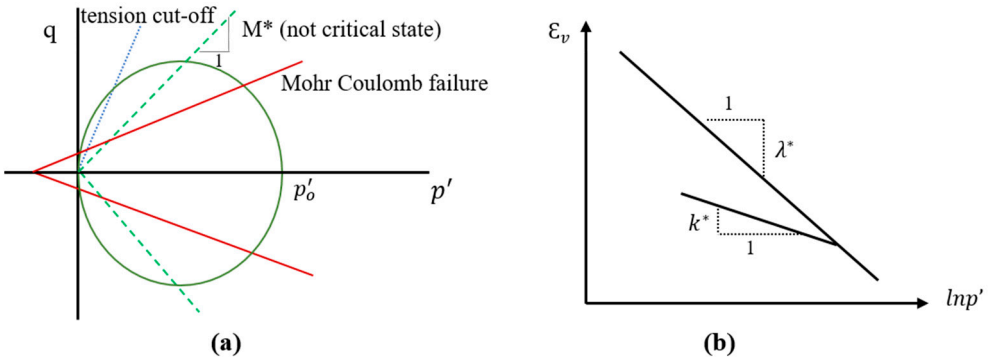

Figure 2. Soft soil model: (**a**) Yield surface; (**b**) Compression behavior [17].

The HS model, a second-order model, is a more demanding and realistic model for deep excavation analysis. It provides realistic wall deflection, a ground settlement profile due to its nonlinearity, inelastic stiffness, and a stress-dependency principle [18]. This model is highly recommended for excavation modeling for both soft and stiff soils. The input parameters for this model consist of three reference stiffness parameters, along with other parameters. They are: stiffness modulus at reference pressure (E_{50}^{ref}) from triaxial compression, the elastic modulus for unloading/reloading at reference pressure (E_{ur}^{ref}) from triaxial unloading/reloading, the stiffness from oedometer loading (E_{oed}^{ref}), a power m, for the stress-dependent stiffness formulation, the pure elastic Poisson's ratio or unloading/reloading Poisson's ratio, ν_{ur}, the Mohr–Coulomb strength parameters (Φ, c), the K_o-value in primary one-dimensional compression (K_{onc}), and the failure ratio [14].

The stiffness modulus E_{50}^{ref} is the secant stiffness at 50% of the maximum deviatoric stress for a reference minor principal effective stress of $\sigma_3' = p^{ref} = 100$ kPa. According to Calvello and Finno [19], the relation of $E_{ur}^{ref} = 3 \times E_{50}^{ref}$ is used to determine the elastic

modulus E_{ur}^{ref} (Figure 3), while E_{oed}^{ref} is evaluated from the consolidation tests as illustrated in Figure 4. In addition, the relation with the modified compression index, λ^*, can be used to determine the E_{oed}^{ref} using the relation mentioned below:

$$E_{oed}^{ref} = \frac{p^{ref}}{\lambda^*}, \ \lambda^* = \frac{\lambda}{1 + e_0} \tag{3}$$

where p^{ref} is a reference pressure.

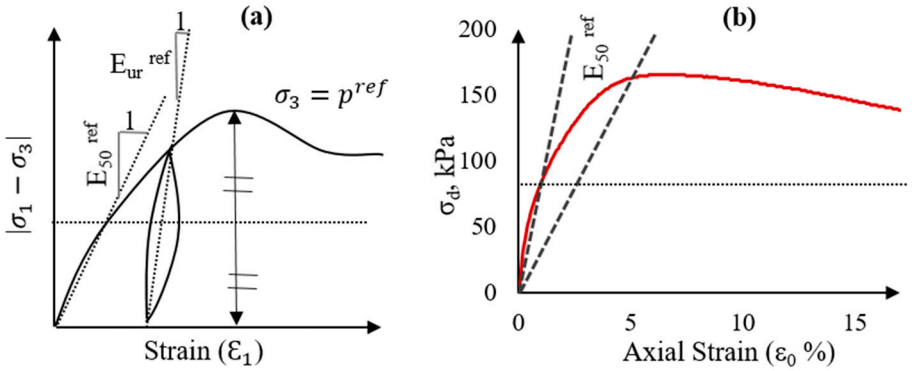

Figure 3. Soil modulus: (**a**) Fundamental concept; (**b**) Secant modulus (E_{50}^{ref}).

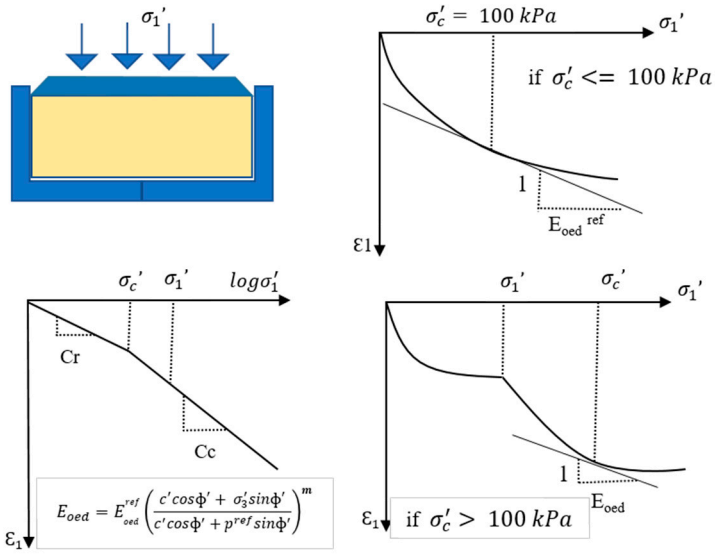

Figure 4. Illustration on the determination of E_{oed}^{ref} [18].

The power of the stress level-dependency of stiffness m, can be determined by plotting $\ln(E_{50})$ vs. $\ln\left(\frac{c'cos\Phi' + \sigma_3' sin\Phi'}{c'cos\Phi' + p_{ref} sin\Phi'}\right)^m$ on a natural scale. The slope of the best fit straight line is the value of m discussed in research [18]. Here, the obtained value of m was close to 1; therefore, it was considered as 1 for simplicity [20] and ν_{ur} was taken as 0.2 [18]. Furthermore, the Mohr–Coulomb strength parameters of the cohesion and friction angle were the same as determined in the MC model.

The HSS model improves the result by considering the small strain characteristics of the soil. The result obtained is more realistic and closer to the field data and gives better results than the HS model [21]. The input parameters used in this model are similar to the HS model except for two additional parameters, i.e., the reference shear modulus at small strain (G_0^{ref}) and shear strain ($\gamma_{0.7}$). The shear strain ($\gamma_{0.7}$) is the strain at which the secant shear modulus

is equal to $0.7G_0^{ref}$. In this study, the reference shear modulus at a small strain (G_0^{ref}) was determined using the Young's modulus at a small strain using Equation (4).

$$G_0^{ref} = E_0^{ref} \ / \ (2 \times (1 + \nu_{ur})) \tag{4}$$

The value of $\gamma_{0.7}$ was determined using the relation given in the PLAXIS manual as

$$\gamma_{0.7} = \frac{1}{9Go}\left[2c'(1 + cos2\Phi') - \sigma_1'(1 + K_o)sin2\Phi'\right] \tag{5}$$

where K_o = the earth pressure coefficient at rest, σ_1' = the effective vertical stress (pressure negative), and

$$G_o = G_o^{ref} \times \left(\frac{c'cos\Phi' + \sigma_3' sin\Phi'}{c'cos\Phi' + p^{ref} sin\Phi'}\right)^m = p^{ref} \tag{6}$$

p^{ref} in Equation (6) is the reference pressure which is considered 100 kPa.

1.2. Numerical Analysis

PLAXIS 2D, a finite element-based software, is widely used in deep excavation analysis [9]. The interaction of soil elements in the model is governed by the stress–strain relationship; therefore, no assumption for the slip surface is required. This also provides a better visualization of the deformation of the soil mass [22]. As mentioned by Schweiger [23], models used in the PLAXIS can be categorized into five parts which have different patterns, i.e., linear or nonlinear elastic models, elastic–perfectly plastic models, isotropic hardening single surface plasticity models, isotropic hardening double surface plasticity models, and kinematic hardening multi-surface plasticity models. The suitability of the models depends on the soil behavior, type of analysis, etc. [24], which is presented in Table 1.

Table 1. Appropriateness of different constitutive soil models for the analysis of soft soils [24].

Constitutive Models	Analysis Type	Soft Soil			
		OCR > 1	OCR ≈ 1	OCR < 1	Sandy Soil
MC Model	Serviceability Limit State				
	Bearing Capacity Limit State	*			**
Modified Cam Clay	Serviceability Limit State		*	*	
	Bearing Capacity Limit State		**	**	
HS Model	Serviceability Limit State	***	**	**	***
	Bearing Capacity Limit State	***	**	**	***

OCR: over consolidation ratio; *: generally applicable, the effect is not ideal; **: applicable, good effect; ***: applicable, very good effect.

The hardening soil (HS) model, an elastic–plastic soil model, is the classical plasticity theory-based model [25]. The HS model is a more acceptable and advanced model in deep excavation analysis which can better simulate real soil behaviors. This model is widely used nowadays because of its capacity to simulate the nonlinear, inelastic, and stress-dependent behavior of soil [18]. Therefore, it predicts a more realistic ground settlement profile and wall deflection, overcoming the shortcomings of the MC model. In addition, it yields a smaller toe movement and bottom heave than the MC model [18]. To obtain a more realistic outcome and enhance the results obtained from the HS model, the HSS model is used more often recently. The HSS model uses a modified hyperbolic law for the stiffness degradation curve [26,27]. It considers the small strain characteristics of the soil, the unloading stiffness, and the strain-dependent stiffness behaviour of the soil. Thus, the result obtained is closer to the field response of ground excavations in soft soils.

Lim et al. [14] performed the evaluation of constitutive soil models in clay under undrained conditions monitoring the support deflection and settlement during the deep excavation at Taipei National Enterprise Center and reported that the HS model results in a slightly higher wall displacement and ground settlement in comparison to the field observation. However, the prediction from the HS model is closer than those from the MC and MCC models. To improve the results from the HS model, the HSS model considers the small strain characteristics of the soil. However, on comparing the results from the HS model and the HSS model, there is no difference in the wall displacement but little improvement in the prediction of surface deformation. Furthermore, a similar result was also obtained by Surarak et al., 2012 [20] on a mass rapid transit (MRT) underground railway. This implies that both models are suitable for the analysis of deep excavation. Similarly, in the same study, the MC model predicted the wall displacement closer to the field measurement only after applying $E_u/S_u = 0$. However, in the early stages, the wall displacement predicted was significantly different from the field measurement. The results from this research are similar to the results obtained by Likitlersuang et al., 2013 [21]. Although the model is mostly used in geotechnical analysis, this is unsuitable to determine the stress state in deep excavation analysis.

Different types of sheet piles like steel sheet piles, precast concrete sheet piles, wooden sheet piles, and aluminum sheet piles are used in various construction and civil engineering projects as the retaining structures like water front structures, bridge abutments, flood controls, retaining walls, underground structures, etc. [28,29]. Cantilever sheet piles rely on lateral passive resistance from the embedment depth, while anchored sheet piles use anchors to reduce the deflection, bending moment, and embedment depth for effective design [30]. The inclination, length, and position of the anchor also have great importance in economic design [31]. The effect of parametric variations in anchor in anchored sheet pile and the effect of embedment depth in the sheet pile are well studied by Pokhrel [32]. A lateral displacement of up to 2% of the maximum depth of excavation is adopted during the stability analysis of underground projects [33–35]. Different types of failure mode in anchored sheet pile walls are represented in FHWA [36]. Similarly, the finite element method is employed in various studies for the analysis of safety, deflection, bending, and stress–strain analysis of sheet piles [19,37–43].

During deep excavation, the pattern of retaining wall displacement is mainly affected by the type of subsoil, support system, workmanship, etc. The wall movement is divided into cantilever or deep inward or braced excavations as per Hsieh and Ou [44] (Figure 5). A cantilever-type movement occurs during the initial stage of excavation or when the subsoil is dominant with sandy soil. Likewise, a deep inward movement is especially seen in soft soils from the initial stage of excavation as mentioned in Refs. [44,45]. According to Hsieh and Ou [44], ground settlement profiles can be categorized as spandrel and concave. In the spandrel settlement, the maximum surface settlement is observed close to the wall, typically when the wall movement follows a cantilever pattern. Meanwhile, the concave ground settlement occurs when there is deep inward movement of the wall, causing the maximum surface settlement to occur at a distance from the wall [45].

In the soil of Kathmandu, many research studies related to deep excavation have been carried out but those studies mainly focused on the parametric variation in the support system using a conservative constitutive model like the MC model. Due to the lack of sufficient data for an advanced constitutive model, the studies were limited to the Mohr–Coulomb model and rarely to the MCC model. Pokhrel [32] performed a parametric analysis on flexible and rigid support systems using the MC model. Likewise, Tiwari [46] conducted a comparison between the MC model and the MCC model. This comparison focused on evaluating the horizontal and vertical deformation of protective piles. However, the rationale for choosing these specific models for the Kathmandu soil was not discussed properly. Despite the suitability evaluation of these constitutive soil models for Kathmandu soil, their parametric analysis for the comparison of pile deformation did not yield reliable results. Similarly, Nyoupane et al. [47] performed numerical modeling of triaxial tests using

some constitutive soil model on secondary data. However, these models did not account for soil behavior under small strains, which is a critical consideration in modeling clay and deep excavations. Additionally, no investigation has been conducted into the effectiveness of these constitutive models in organic soil. As a result, it is crucial to evaluate different soil constitutive models and compare the ground response predictions that appropriately incorporate various soil behaviors with actual ground responses for future applications.

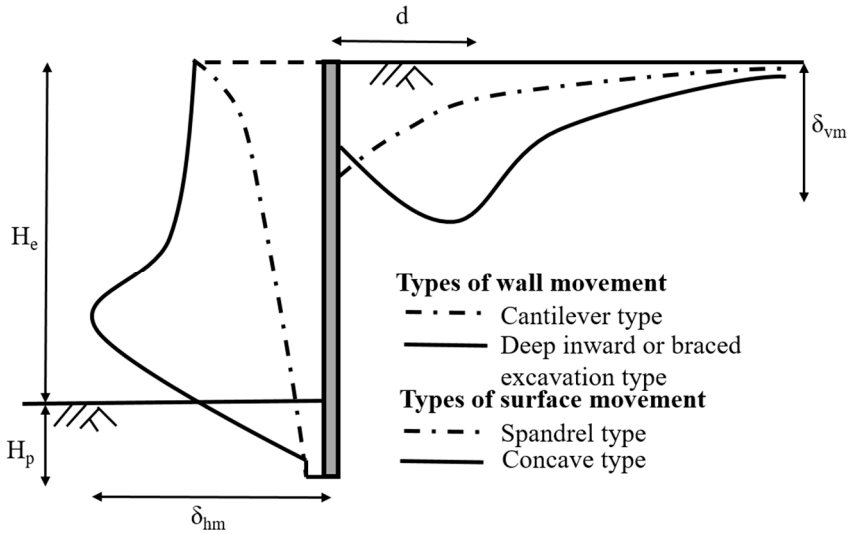

Figure 5. Types of wall movement and ground surface settlement (after Hsieh and Ou [45]).

2. Materials and Methods

2.1. Materials

Tukucha (an area at the confluence Bagmati River and Tukucha Stream) was selected for soil sampling, which is located in between the Bagmati River and the Department of Passport in Tripureshwor, Kathmandu. This area is in the middle of Kathmandu Valley and has the typical geological and geotechnical characteristics of Kathmandu Valley. Kathmandu Valley lies within the broader Himalayan region, which began forming around 50 million years ago due to the collision between the Indian Plate and the Eurasian Plate. This collision resulted in the uplift of the Himalayan Range [48,49]. During the early stages of the Himalayas' formation, sedimentation was prominent in Kathmandu Valley area. Rivers transported sediments from the rising mountains and deposited them in basins, including Kathmandu Valley, which began to take shape as a structural basin [50]. As the Himalayas continued to rise and rivers continued to deposit sediments during different geological epochs, the lake eventually got filled with sediments, forming the present-day landscape of the valley. Tukucha features clayey lacustrine deposits; however, the upper shallow alluvial deposits are deposited by Bagmati River and Tukucha River.

The soil profile of the site consists of a surficial soil layer up to 2 m in depth, which contains waste materials such as cotton clothes, plastic bags, sand with silty clay, etc, while the remaining layers are dark gray, medium-stiff to stiff organic soil of medium-to-high plasticity.

Undisturbed samples were collected from 4.5 m, 9 m, and 12 m depths of different boreholes using Shelby tubes and the disturbed sample from the standard penetration tests. The sampling tube was waxed to prevent moisture exchange and taken to the soil lab for further testing. Tests like particle size distribution, Atterberg's limits, specific gravity, natural moisture content, bulk unit weight, and the consolidated undrained (CU) triaxial test, were performed in Heavy Lab, Institute of Engineering, Pulchowk Campus, Lalitpur, Nepal. Furthermore, one dimensional consolidation test was executed in the Central Material Testing Laboratory (CMTL), Institute of Engineering, Pulchowk Campus, Lalitpur, Nepal.

2.2. Experimental Equipment and Test Procedure

The Atterberg limits tests were conducted according to ASTM D4318 [51]. The specific gravity test was conducted according to ASTM D854 [52] using a Water Pycnometer. The natural moisture content test was conducted according to the ASTM D2216 [53] standard. The consolidated undrained (CU) triaxial test, following the ASTM D4767 [54] standard test method, was performed to determine the strength parameters. From each layer of soil collected in the field, three cylindrical samples of 38 mm in diameter and 76 mm in length were used to conduct consolidated undrained (CU) triaxial tests. The cylindrical remolded samples were trimmed to the desired dimensions and then each sample was encased in a rubber membrane and wrapped with a filter strip. After ensuring stability, the sample was mounted onto a pedestal with a top cap secured by an O-ring. After that, the sample, enclosed within the cell, was immersed in water. Cell pressure was applied using a hydromatic system, allowing the sample to undergo saturation, consolidation, and monotonic shear phases. Tests were performed in three stages, i.e., saturation, isotropic consolidation, and a shearing phase, varying an effective consolidation pressure of 50, 100, 200, and 400 kPa. Eventually, by varying the consolidation pressure across different samples, the shear strength parameters were analyzed to assess the strength characteristics of the soil.

2.3. Parameters for Numerical Simulation

The parameters required for different constitutive models for numerical analysis were determined as discussed in the earlier section. These parameters were utilized to model the soil in PLAXIS 2D for finite element analysis (FEA) (Figure 6). The FEA results were then compared with the stress–strain relationships obtained from laboratory tests. The model that yielded results close to the laboratory results was used as a reference model for the comparison with different models.

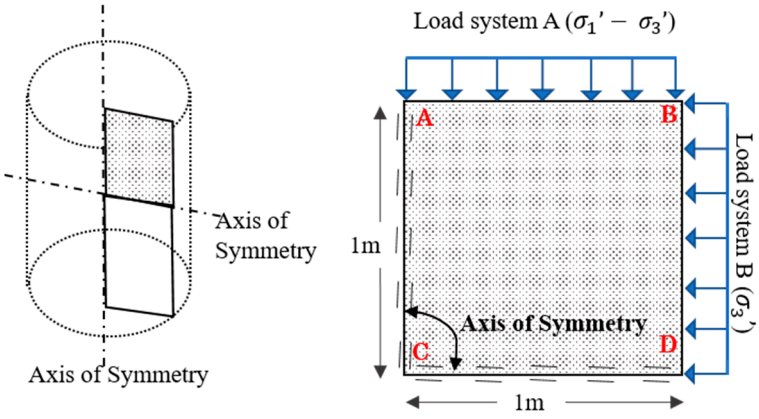

Figure 6. Simplified geometries of triaxial test in FEM models [20].

For the deep excavation analysis, the geometric and material parameters employed are presented in Figure 7 and Table 2. The mechanical properties of soil layers including the ones obtained from tests (modulus of elasticity, effective cohesion, effective angle of friction) are presented in subsequent sections.

A section of 100 m wide and 30 m deep, with different soil layers, was considered for analysis (Figure 7a). The excavation of 10 m deep and 20 m wide was carried out in three distinct stages, and anchored sheet pile walls were applied as a retaining structure. The input properties, geometry, boundary conditions, mesh, and calculations were performed in the software as illustrated in Figure 7b,c.

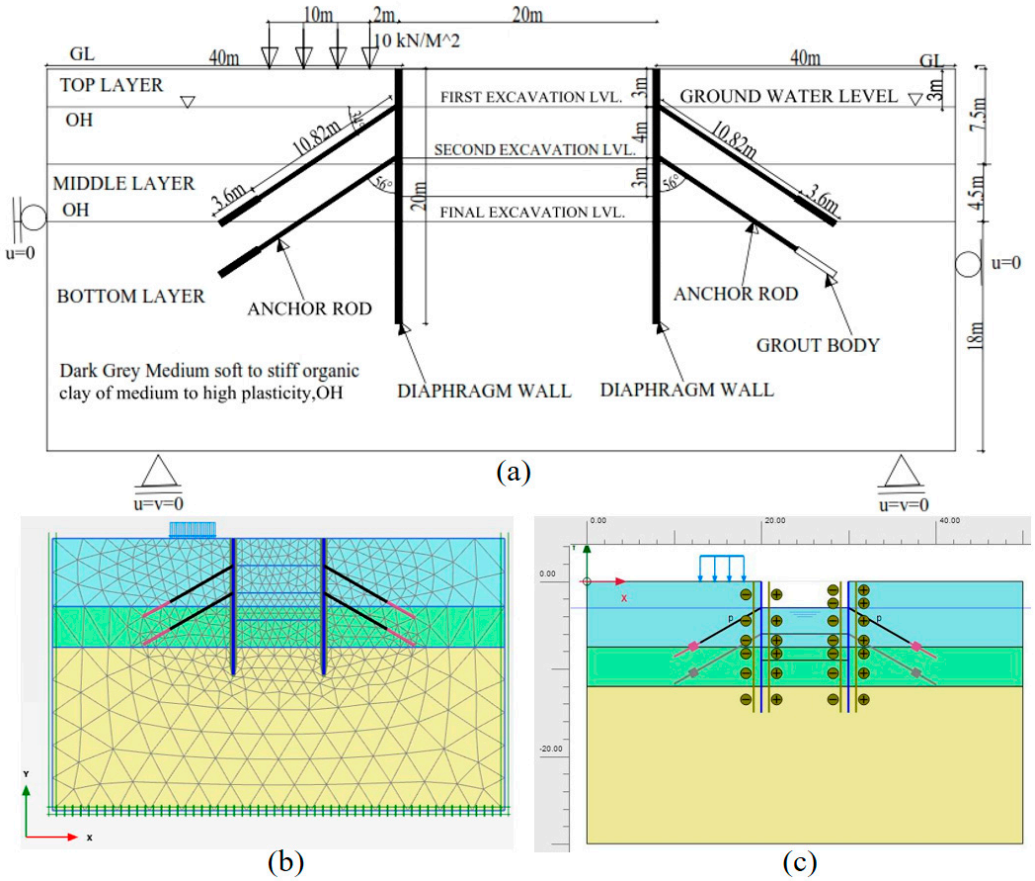

Figure 7. (**a**) Model geometry; (**b**) Meshing; (**c**) Excavation and support systems.

Table 2. Geometric and material properties of the support system.

Parameter		Value	Unit
Size of model		100 × 30	m × m
Depth of excavation		−10	m
Width of excavation		20	m
Load from excavator during excavation		10	kN/m/m
a. Diaphragm Wall			
Length of diaphragm wall		20	m
Material type	-	Elastic, Isotropic	
Normal stiffness	EA	1.2×10^7	kN/m
Flexural rigidity	EI	1.2×10^5	kN m^2/m
b. Anchor Rod			
Depth at anchor placed from ground		3, 7	m
Length of anchor		10.82	m
Angle of anchor with horizontal		34	degree
Material type	-	Elastic, Isotropic	
Normal stiffness	EA	5×10^5	kN
Spacing out of plane	Ls	2.50	m
c. Grout Body			
Length of grout body		3.6	m
Material type	-	Elastic	
Stiffness	E	7.07×10^7	kN/m^2
Diameter	D	0.30	m
Pile spacing	$L_{spacing}$	2.50	m
Skin resistance	$T_{skin.start.max}$	400.00	kN/m
	$T_{skin.end.max}$	400.00	kN/m

3. Results

3.1. Evaluation of Constitutive Model

Table 3 presents the parameters used in the MC model. Poisson's ratio was determined by the trial and error method to obtain a realistic value of K_o, which ranges from 0.3 to 0.4 [15]. However, the value of υ is in the range of 0.15 to 0.25 for unloading conditions. Furthermore, the effective cohesion ($C^{'}$) and effective friction angle ($\Phi^{'}$) were used in the modeling. The dilatancy angle is negligible in the soil; therefore, the value was taken as zero which complies with the condition $\Psi = \Phi - 30^{\circ}$ [15].

Table 3. Input parameters for the MC model.

Depth (m)	Young's Modulus (E) [kN/m^2]	Poisson's Ratio (ν)	Effective Cohesion (c′) [kN/m^2]	Friction Angle (Φ′) [°]	Dilatancy Angle (Ψ) [°]	Permeability	
						K_x [m/day]	K_y [m/day]
0–7.5	13235.4	0.30	53.0	13.86	-	1.69×10^{-4}	1.69×10^{-4}
7.5–12	1733.9	0.30	62.0	16.70	-	9.94×10^{-5}	9.94×10^{-5}
>12.0	22490.6	0.30	58.0	19.43	-	1.24×10^{-4}	1.24×10^{-4}

Similarly, the input parameters for different constitutive models are presented in Tables 4 and 5. The SS model requires the modified compression index (λ*), the modified swelling index (k*), and the Mohr–Coulomb failure parameters ($c^{'}$, $\Phi^{'}$, Ψ) as presented in Table 4. The swelling index was taken as equivalent to recompression. The ratio λ^*/k^* $(= \lambda/k)$ varies from 3 to 6 [55], and the value found in this study was consistent with this range.

Table 4. Input parameters for the soft soil (SS) model.

Depth (m)	Modified Compression Index λ*	Modified Swelling Index k*	Effective Cohesion c′ [kN/m^2]	Friction Angle Φ′ [°]	Dilatancy Angle Ψ [°]
0–7.5	0.080	0.017	53.0	13.86	-
7.5–12	0.049	0.007	62.0	16.70	-
>12.0	0.041	0.007	58.0	19.43	-

Table 5. Input parameters for the hardening soil (HS) model.

Depth [m]	E_{50}^{ref} [kN/m^2]	E_{oed}^{ref} [kN/m^2]	E_{ur}^{ref} [kN/m^2]	m	Effective Cohesion, c' [kN/m^2]	Friction Angle, Φ' [°]
0–7.5	8645.8	11,440.0	25,937.5	1.0	53.0	13.86
7.5–12	4384.6	4865.0	13,153.8	1.0	62.0	16.70
>12.0	12,840.9	12,841.0	38,522.7	1.0	58.0	19.43

Table 5 presents the input parameters for the HS model, including additional parameters from the loading and unloading behavior of soil from the one-dimension consolidation tests. For the HSS model, the input parameters are similar to the HS model except for two additional parameters, i.e., the reference shear modulus at minor strain ($G0_{ref}$) and shear strain ($\gamma_{0.7}$), as presented in Table 6.

Table 6. Input parameters for the hardening soil small strain (HSS) model.

Depth [m]	E_{50}^{ref} [kN/m^2]	E_{oed}^{ref} [kN/m^2]	E_{ur}^{ref} [kN/m^2]	m	G_0^{ref} (Calculated) [kN/m^2]	G_0^{ref}	$\gamma_{(0.7)}$
0–7.5	8645.8	11,440.0	25,937.5	1.0	6172.8	11,239.6	8.9×10^{-4}
7.5–12	4384.6	4865.0	13,153.8	1.0	3418.8	5700.0	1.1×10^{-3}
>12.0	12,840.9	12,841.0	38,522.7	1.0	6089.7	16693.2	1.6×10^{-3}

The results of the numerical analysis of triaxial compression tests were compared with the laboratory tests to determine the most suitable constitutive model. As presented in Figure 8, the stress–strain curves obtained from the HS and the HSS models were closer to most of the laboratory tests, consistent with the previous study's result [47]. Furthermore, the HSS model predicts more accurately, as shown in Figure 8, because it considers the small strain characteristics of soils, as mentioned in the different literature [14,21,56].

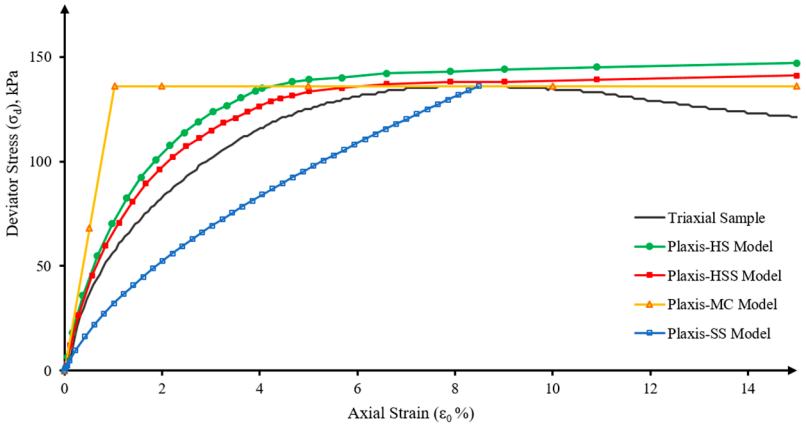

Figure 8. Comparison of stress–strain behaviors from PLAXIS and a laboratory test.

3.2. Ground Response Analysis

Since the results from the HSS model most accurately reflected the laboratory test outcomes, the HSS model was deemed to accurately represent the real ground behavior during excavation. Therefore, the wall deformation and ground settlement profiles obtained from the HSS model are used as a reference for comparison of the results obtained from the other models.

During the first, second, and final excavation stages, the maximum wall deflection occurs at different depths, such as 5 m, 7 m, and 9 m below the ground surface. Meanwhile, the deflection profile decreases significantly at the base of the diaphragm wall (see Figure 9a). Similarly, considerable ground settlement is seen near the wall, with the settlement increasing and reaching its maximum value within 5 to 10 m from the wall (Figure 9b). This indicates that deep excavation has the most pronounced impact close to the wall and diminishes significantly as the distance increases. The study's deflection and ground settlement patterns align with previous studies [21,44,57,58].

Figure 10 illustrates the comparison between the wall deflection and ground settlement profiles obtained from the MC and HSS models. In Figure 10a, it is illustrated that the wall deflection during the initial excavation stages exceeds the predictions made by the HSS model. However, the predicted wall deflection was lower during the final excavation stage. Likewise, the ground settlement profiles in the initial stages of excavations were slightly higher than anticipated by the HSS model, while the settlement profiles showed significantly lower values during the final excavation stage (Figure 10b). It is worth noting that this increased difference in ground settlement with excavation depth aligns with findings from previous studies [14,21,56].

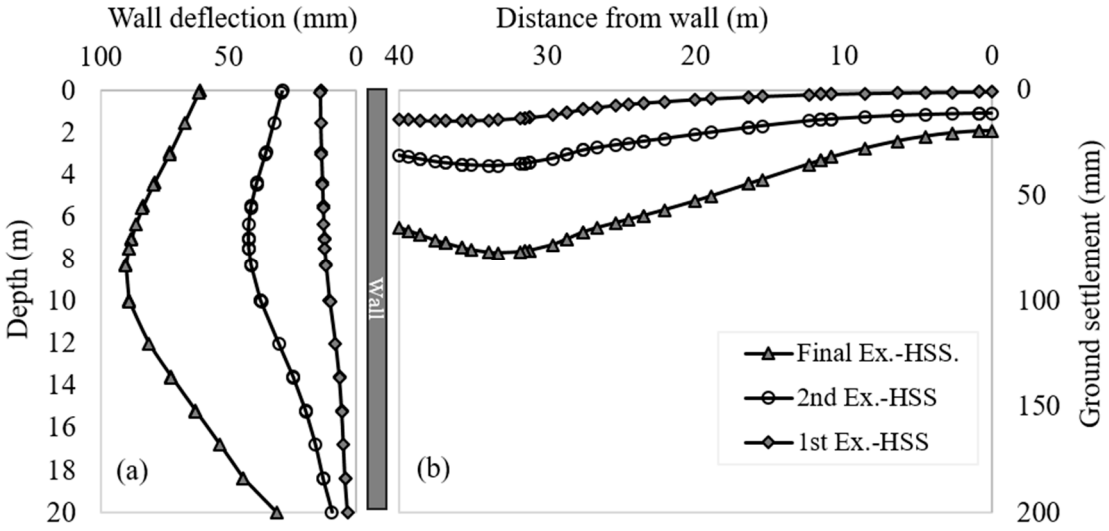

Figure 9. Ground response obtained using the HSS model. (**a**) Wall deflection; (**b**) Ground settlement profile.

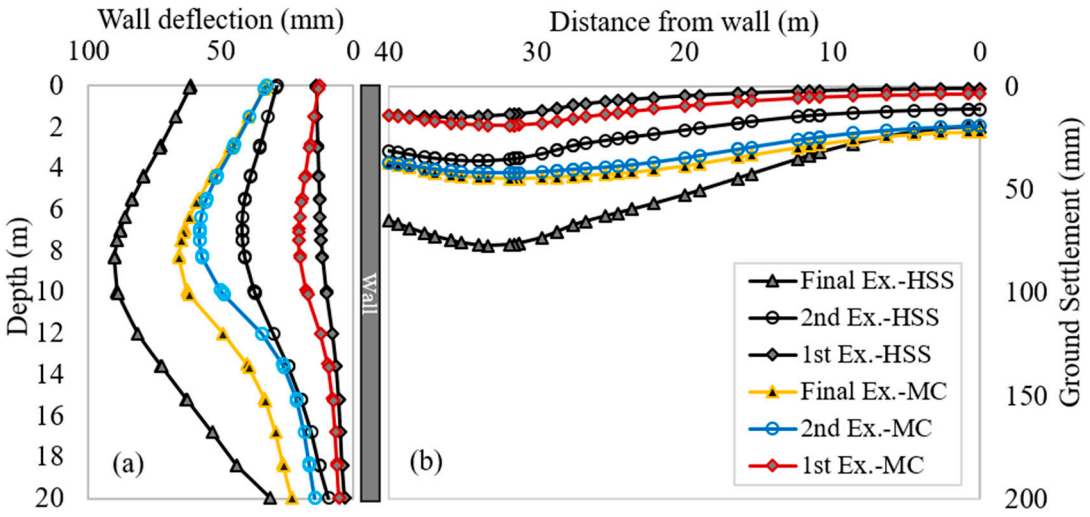

Figure 10. Comparison of (**a**) wall deflection and (**b**) the ground settlement profile from the MC and HSS models.

Figure 11 depicts the results from the SS and HSS models. In Figure 11a, it is evident that the wall deflection determined by the SS model is notably smaller than that of the HSS model. Similarly, in Figure 11b, the ground settlement profiles obtained from the SS model are significantly lower than those obtained from the HSS model. Consequently, the predictions of wall deflection and ground settlement profiles from this model might be overly optimistic and substantially underestimated for deep excavations in typical Kathmandu soil.

During the initial stages of excavation, the wall deflection determined by the HS model closely aligned with the predictions from the HSS model, as shown in Figure 12a. Furthermore, in the final excavation stage, the wall deflection obtained from the HS model was slightly lower than the HSS model. Similar results were also observed in the ground settlement profiles, as shown in Figure 12b. This suggests that both the HS and HSS models produce similar predictions. This pattern of wall deflections and ground settlement profiles aligns with the results reported in previous studies [23,59]. However, the inclusion of the small strain characteristics of soil in the HSS model impacts the prediction accuracy, which is consistent with the findings of previous studies [14,21].

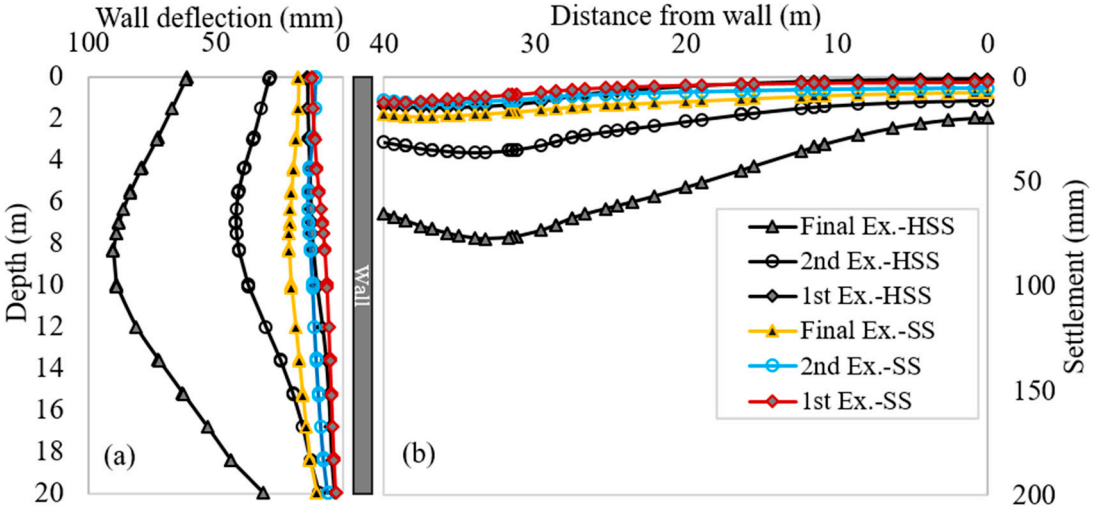

Figure 11. Comparison of (**a**) wall deflection and (**b**) the ground settlement profile from the SS and HSS models.

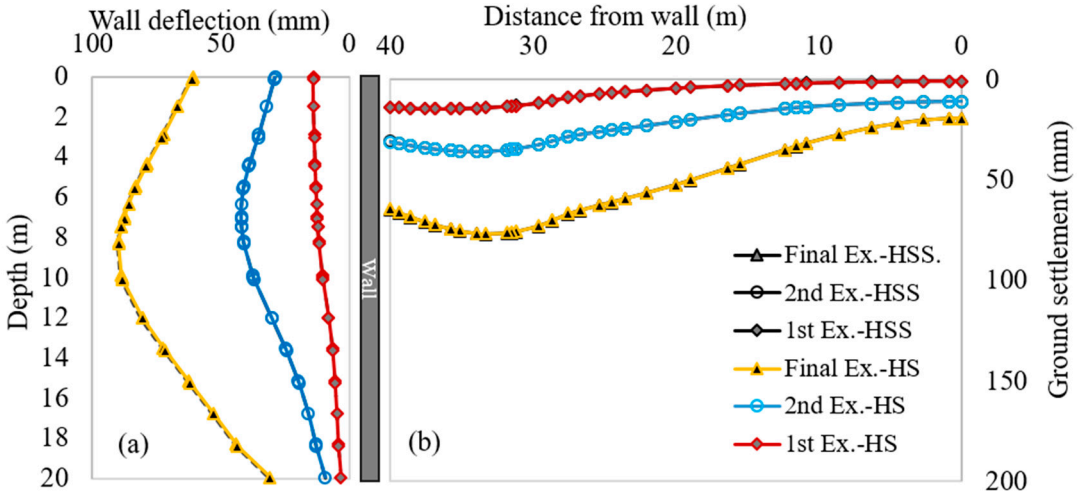

Figure 12. Comparison of (**a**) wall deflection and (**b**) the ground settlement profile from the HS and HSS models.

4. Conclusions

This study highlights the significance of selecting an appropriate constitutive model for enhancing the efficiency of deep excavation support systems in the lacustrine deposits of Kathmandu Valley. The research findings indicate that the HSS model is the most suitable choice for modeling Kathmandu soil. It accurately predicts mechanical behavior and closely fits with laboratory test results. The key findings can be summarized as follows:

- Wall deflection is seen near the ground surface, gradually increasing with excavation depth and decreasing significantly towards the end of the diaphragm wall. In the final excavation stage, the wall deflection values obtained from the MC, SS, and HS models are 22%, 77%, and 0.1% lower than that obtained from the HSS model, respectively.
- Similarly, ground settlement increases from the wall to a certain distance and then decrease further away from the wall. The maximum ground settlement from the MC, SS, and HS models are 46%, 76%, and 0.09% lower than predicted by HSS models, respectively.
- The HS model yields results similar to the HSS model, reinforcing its suitability for analyzing Kathmandu soil. While the MC and SS models predict significantly lower values for both maximum wall deflection and ground surface deformation, caution

is advised when using these models to analyze deep excavation support systems in Kathmandu Valley.

These findings underscore the importance of selecting the appropriate constitutive model for proper analysis of deep excavation. Additionally, the study acknowledges its limitations, particularly in the modeling of in situ soil behavior, support systems, and their interactions, suggesting the need for field measurements and monitoring during actual excavation processes to improve the realism of the analysis.

Author Contributions: Conceptualization, B.K.D.; Methodology, B.K.D., S.R. and K.P.; Software, B.K.D., S.R., D.D. and K.P.; Validation, B.K.D. and S.R.; Formal analysis, B.K.D., S.R., D.D. and D.K.; Investigation, B.K.D., K.P., D.D. and D.K.; Resources, B.K.D.; Data curation, B.K.D., S.R. and D.K.; Writing—original draft, B.K.D. and S.R.; Writing—review & editing, B.K.D. and D.K.; Visualization, B.K.D. and D.K.; Supervision, B.K.D.; Project administration, B.K.D. All authors have read and agreed to the published version of the manuscript.

Funding: No funding was received for conducting this study.

Data Availability Statement: The authors will make the data and materials that support the results or analyses presented in this paper freely available upon request.

Acknowledgments: The author(s) would like to thank Department of Civil Engineering, Pulchowk Campus, Institute of Engineering, Tribhuvan University, for providing resources to complete this research.

Conflicts of Interest: Diwakar KC is employed by the company Geotechnology LLC. The remaining authors declare that the research was conducted in the absence of any commercial or financial relationships that could be construed as a potential conflict of interest.

References

1. Dahal, R.K.; Aryal, A. Geotechnical properties of soil in Sundhara and Jamal. *J. Nepal. Geol. Soc.* **2002**, *27*, 77–86.
2. Katel, T.P.; Upreti, B.N.; Pokharel, G.S. Engineering properties of fine grained soils of Kathmandu Valley, Nepal. *J. Nepal. Geol. Soc.* **1996**, *13*, 121–138. [CrossRef]
3. Koirala, A.; Shrestha, O.; Karmacharya, R. Engineering geology of the southern part of Kathmandu Valley. *J. Nepal. Geol. Soc.* **1993**, *3*, 151–159.
4. Setopati. *Houses Subside Due to under—Construction Summit Apartment*; Setopati: Lalitpur, Nepal, 2023.
5. Thoker, K. *Road Caves in at Naxal, Execssive Digging for Hotel Construction Blamed*; My Repub: Kathmandu, Nepal, 2017.
6. Dahal, B.K.; Zheng, J.J.; Zhang, R.J. Experimental investigation on physical and mechanical behavior of Kathmandu clay. *Adv. Mater. Res.* **2018**, *1145*, 112–116. [CrossRef]
7. Atkinson, J.; Sallfors, G. Experimental determination of soil properties. In Proceedings of the 10th ECSMFE, Florence, Italy, 26–30 May 1991; Volume 3, pp. 915–956.
8. Aung, Y.; Khabbaz, H.; Fatahi, B. Mixed hardening hyper-viscoplasticity model for soils incorporating non-linear creep rate—H-creep model. *Int. J. Plast.* **2019**, *120*, 88–114. [CrossRef]
9. Bhatkar, T.; Barman, D.; Mandal, A.; Usmani, A. Prediction of behaviour of a deep excavation in soft soil: A case study. *Int. J. Geotech. Eng.* **2017**, *11*, 10–19. [CrossRef]
10. Nguyen, L.; Fatahi, B. Behaviour of clay treated with cement & fibre while capturing cementation degradation and fibre failure—C3F Model. *Int. J. Plast.* **2016**, *81*, 168–195.
11. Vukadin, V.; Jovičić, V. S_BRICK: A constitutive model for soils and soft rocks. *Acta Geotech. Slov.* **2018**, *15*, 16–37. [CrossRef]
12. Wang, W.D.; Wang, H.R.; Xu, Z.H. Experimental study of parameters of hardening soil model for numerical analysis of excavations of foundation pits. *Rock Soil Mech.* **2012**, *33*, 2283–2290.
13. Zou, C.; Wang, Y.; Lin, J.; Chen, Y. Creep behaviors and constitutive model for high density polyethylene geogrid and its application to reinforced soil retaining wall on soft soil foundation. *Constr. Build. Mater.* **2016**, *114*, 763–771. [CrossRef]
14. Lim, A.; Ou, C.Y.; Hsieh, P.G. Evaluation of clay constitutive models for analysis of deep excavation under undrained conditions. *J. Geoengin.* **2010**, *5*, 9–20. [CrossRef]
15. PLAXIS 2D. *Reference Manual*; Bentley Communities: Exton, PA, USA, 2021.
16. Karstunen, M.; Amavasai, A. *Best Soil: Soft Soil Modelling and Parameter Determination*; Chalmers University of Technology: Gothenburg, Sweden, 2017.
17. PLAXIS 2D. *Material Models Manual 2D*; Bentley Communities: Exton, PA, USA, 2021.
18. Teo, P.; Wong, K. Application of the Hardening Soil model in deep excavation analysis. *IES J. Part A Civ. Struct. Eng.* **2012**, *5*, 152–165. [CrossRef]
19. Calvello, M.; Finno, R.J. Selecting parameters to optimize in model calibration by inverse analysis. *Comput. Geotech.* **2004**, *31*, 410–424. [CrossRef]

20. Surarak, C.; Likitlersuang, S.; Wanatowski, D.; Balasubramaniam, A.; Oh, E.; Guan, H. Stiffness and strength parameters for hardening soil model of soft and stiff Bangkok clays. *Soils Found.* **2012**, *52*, 682–697. [CrossRef]
21. Likitlersuang, S.; Surarak, C.; Wanatowski, D.; Oh, E.; Balasubramaniam, A. Finite element analysis of a deep excavation: A case study from the Bangkok MRT. *Soils Found.* **2013**, *53*, 756–773. [CrossRef]
22. Dhakal, D. Slope Stability Analysis of Hill Side Steep Cut Slope and Its Stabilization by the Method of Soil Nailing Technique: A Case Study on Narayanghat—Mugling Road Section. In Proceedings of the IOE Graduate Conference, Lalitpur, Nepal, 24–25 May 2019.
23. Schweiger, H.F. Influence of constitutive model and EC7 design approach in FE analysis of deep excavations. In Proceedings of the ISSMGE Int. Seminar on Deep Excavations and Retaining Structures, Budapest, Hungary, 4–5 February 2009; pp. 99–114.
24. Fu, Y.; He, S.; Zhang, S.; Yang, Y. Parameter Analysis on Hardening Soil Model of Soft Soil for Foundation Pits Based on Shear Rates in Shenzhen Bay, China. *Adv. Mater. Sci. Eng.* **2020**, *2020*, 7810918. [CrossRef]
25. Brinkgreve, R.B. Plaxis Version 9 Material Model Manual. Plaxis bv: Delft, The Netherlands, 2004.
26. Hardin, B.O.; Drnevich, V.P. Shear modulus and damping in soils: Design equations and curves. *J. Soil Mech. Found. Div.* **1972**, *98*, 667–692. [CrossRef]
27. Santos, J.A.; Correia, A.G. Reference Threshold shear strain of soil, its application to obtain a unique strain dependent shear modulus curve for soil. In Proceedings of the 15th Inetrnational Conference on Soil Mechanics and Geotechnical Engineering, Istanbul, Turkey, 27–31 August 2001; Volume 1, pp. 267–270.
28. Bilgin, Ö. Numerical studies of anchored sheet pile wall behavior constructed in cut and fill conditions. *Comput. Geotech.* **2010**, *37*, 399–407. [CrossRef]
29. Dawkins, W. *Investigation of Wall Friction, Surcharge Loads, and Moment Reduction Curves for Anchored Sheet-Pile Walls*; US Army Corps of Engineers: Houston, TX, USA, 2001.
30. Das, B.M. *Advanced Soil Mechanics*; CRC Press, Taylor and Francis Group: Boca Raton, FL, USA; New York, NY, USA, 2019.
31. Bilgin, Ö. Lateral Earth Pressure Coefficients for Anchored Sheet Pile Walls. *Int. J. Géoméch.* **2012**, *12*, 584–595. [CrossRef]
32. Pokhrel, S. *Parametric Analysis of Flexible and Rigid Excavation Support System*; Insitute of Engineering, Pulchowk Campus, Tribhuvan University: Lalitpur, Nepal, 2022.
33. Ou, C.-Y.; Hsieh, P.-G.; Chiou, D.-C. Characteristics of ground surface settlement during excavation. *Can. Geotech. J.* **1993**, *30*, 758–767. [CrossRef]
34. Long, M. Database for retaining wall and ground movements due to deep excavations. *J. Geotech. Geoenvironmental Eng.* **2001**, *127*, 203–224. [CrossRef]
35. Moormann, C. Analysis of Wall and Ground Movements Due to Deep Excavations in Soft Soil Based on a New Worldwide Database. *Soils Found.* **2004**, *44*, 87–98. [CrossRef]
36. FHWA. *Geotechnical Engineering Circular No. 4: Ground Anchors and Anchored Systems*; Federal Highway Administration: Washington, DC, USA, 1999.
37. Bahrami, M.; Khodakarami, M.I.; Haddad, A. 3D numerical investigation of the effect of wall penetration depth on excavations behavior in sand. *Comput. Geotech.* **2018**, *98*, 82–92. [CrossRef]
38. Cherubini, C. Probabilistic approach to the design of anchored sheet pile walls. *Comput. Geotech.* **2000**, *26*, 309–330. [CrossRef]
39. Emarah, D.A.; Seleem, S.A. A numerical study of anchored sheet piles subjected to different types of sandy soils backfill. *HBRC J.* **2018**, *14*, 422–430. [CrossRef]
40. Grande, L.; Soreide, O.K.; Tefera, T.H. Large scale model testing on the moment distribution and deformation behaviour of a sheet pile wall. In Proceedings of the 2nd International Conference on Soil Structure Interaction in Urban Civil Engineering, Zurich, Switzerland, 7–8 March 2002; pp. 389–394.
41. GuhaRay, A.; Baidya, D.K. Reliability-based analysis of cantilever sheet pile walls backfilled with different soil types using the finite-element approach. *Int. J. Géoméch.* **2015**, *15*, 6015001. [CrossRef]
42. Han, J.-Y.; Zhao, W.; Chen, Y.; Jia, P.-J.; Guan, Y.-P. Design Analysis and Observed Performance of a Tieback Anchored Pile Wall in Sand. *Math. Probl. Eng.* **2017**, *2017*, 8524078. [CrossRef]
43. Kumar, N.; Dey, A. Behavior of Rigid Cantilever Sheet Pile Walls: Numerical and Finite Element Analysis. In Proceedings of the Indian Geotechnical Conference, Kakinada, India, 19–21 December 2014; pp. 18–20.
44. Hsieh, P.-G.; Ou, C.-Y. Shape of ground surface settlement profiles caused by excavation. *Can. Geotech. J.* **1998**, *35*, 1004–1017. [CrossRef]
45. Ou, C.-Y. *Deep Excavation: Theory and Practice*; CRC Press, Taylor and Francis Group: Boca Raton, FL, USA, 2014.
46. Poudel, P.; Acharya, I.P.; Yadav, S.K. Investigation of Base Stability for an Underground Kathmandu Metro Station. In Proceedings of the 10th IOE Graduate Conference, Kathmandu, Nepal, 30 September–2 October 2021.
47. Nyoupane, K.; Kumar, S.; Prasad, I. Numerical Modelling of Triaxial Tests for Kathmandu Soils. In Proceedings of the 10th IOE Graduate Conference, Kathmandu, Nepal, 30 September–2 October 2021; pp. 734–739.
48. Lyell, C. *Principles of Geology: Or the Modern Changes of the Earth and Its Inhabitants Considered as Illustrative of Geology*; D. Appleton & Company: Boston, MA, USA, 1864.
49. Marshak, S. *Earth: Portrait of a Planet: Fourth International Student Edition*; WW Norton & Company: New York, NY, USA, 2011.
50. Hodges, K.V.; Wobus, C.; Ruhl, K.; Schildgen, T.; Whipple, K. Quaternary deformation, river steepening, and heavy precipitation at the front of the Higher Himalayan ranges. *Earth Planet. Sci. Lett.* **2004**, *220*, 379–389. [CrossRef]

51. *ASTM D4318*; Standard Test Methods for Liquid Limit, Plastic Limit, and Plasticity Index of Soils. ASTM International: West Conshohocken, PA, USA, 2010. [CrossRef]
52. *ASTMD854*; D854—Standard Test Methods for Specific Gravity of Soil Solids by Water Pycnometer. ASTM International: West Conshohocken, PA, USA, 2000. [CrossRef]
53. *ASTMD2216*; Standard Test Methods for Laboratory Determination of Water (Moisture) Content of Soil and Rock by Mass. ASTM International: West Conshohocken, PA, USA, 2010. [CrossRef]
54. *ASTMD4767*; Standard Test Method for Consolidated Undrained Triaxial Compression Test for Cohesive Soils. ASTM International: West Conshohocken, PA, USA, 2003. [CrossRef]
55. Pedro, A.C.G.; Eduardo, P.M.; Jesus, P.J. Engineering Properties of the Coal Ashes stored in the "Valdeserrana" Lagoon. Andorra Power Plant (Spain). *Stud. Environ. Sci.* **1997**, *71*, 167–173. [CrossRef]
56. Ou, C.Y. 2015 TGS geotechnical lecture: Finite element analysis of deep excavation problems. *J. Geoengin.* **2016**, *11*, 1–12. [CrossRef]
57. Tanoli, A.Y.; Yan, B.; Xiong, Y.-L.; Ye, G.-L.; Khalid, U.; Xu, Z.-H. Numerical analysis on zone-divided deep excavation in soft clays using a new small strain elasto–plastic constitutive model. *Undergr. Space* **2022**, *7*, 19–36. [CrossRef]
58. Ou, C.-Y.; Hsieh, P.-G. A simplified method for predicting ground settlement profiles induced by excavation in soft clay. *Comput. Geotech.* **2011**, *38*, 987–997. [CrossRef]
59. Kung, G.T.-C.; Hsiao, E.C.-L.; Juang, C.H. Evaluation of a simplified small-strain soil model for analysis of excavation-induced movements. *Can. Geotech. J.* **2007**, *44*, 726–736. [CrossRef]